# Micromachining of borosilicate glass surfaces using femtosecond higher-order Bessel beams

**Weibo Cheng and Pavel Polynkin***

*College of Optical Sciences, The University of Arizona, 1630 East University Boulevard, Tucson, Arizona 85721, USA*
**Corresponding author: ppolynkin@optics.arizona.edu*

Received September 3, 2014; revised October 4, 2014; accepted October 7, 2014;
posted October 7, 2014 (Doc. ID 221427); published October 29, 2014

We report experimental results on micromachining of borosilicate glass slides with femtosecond higher-order Bessel beams. Transverse intensity profiles of these beams comprise concentric rings that are maintained over extended linear focus zones, facilitating machining geometries with large working distances and high aspect ratios. Both single-shot and multi-shot front-surface machining and multi-shot back-surface processing are experimentally investigated. Material removal in the latter case is furnished through the immersion of the back side of the glass slide in water. Under certain conditions, we observe evidence of self-focusing and azimuthal breakup of the initially smooth ring intensity features of the beams near the glass–water interface. These beam dynamics result in the formation of beaded ring features on the back surface of the glass slide. In the case of multi-shot front-surface machining, pillar-like structures can be fabricated. 

*OCIS codes:* (140.3300) Laser beam shaping; (140.3390) Laser materials processing; (320.7110) Ultrafast nonlinear optics.
http://dx.doi.org/10.1364/JOSAB.31.000C48

## 1. INTRODUCTION

Femtosecond laser micromachining has became ubiquitous in a wide variety of applications such as microfluidics [1], writing optical waveguides [2], and optical data storage [3]. With the help of beam shaping techniques, various exotic beam shapes can be generated and used for laser micromachining. A simultaneous application of both amplitude and phase modulation of the transverse beam profile allows, in principle, for the generation of an arbitrary intensity distribution of the optical field on the material surface. Amplitude modulation, however, is associated with optical loss, which can be undesirable. Yet many practically relevant beam shapes can be produced through phase-only modulation of the beam. Such beam shapes include Bessel, vortex, and Airy beams.

Bessel beams were introduced to optics over 50 years ago by McLeod [4]. The transverse beam profile of a Bessel beam comprises a narrow intensity spike on the beam axis, surrounded by concentric rings. Peak optical intensity of the central spike is maintained over an extended propagation distance, called the linear focus zone, due to a constant inflow of energy from the rings into the central intensity feature. The propagation appears to be diffraction-free relative to the case of an ordinary Gaussian beam with the same width as that of the main intensity spike of the Bessel beam [5]. The diffraction-free feature of Bessel beams has been recently applied to writing channels with high aspect ratios in glass [6].

An optical vortex is another example of a beam that can be generated through phase-only modulation of the initially smooth input beam profile [7]. Since their introduction in the 1990s, vortex beams have been applied in diverse areas such as particle trapping [8] and laser tweezers [9]. Recently, the use of vortex laser beams in surface micromachining has been reported [10]. It has been shown that, under certain conditions, the interaction of a vortex beam with a material surface can drive an implosive axial shock wave resulting in an enhanced damage on the beam axis, where optical intensity is zero. Vortices of low vorticity order of 1 or 2 have been typically used.

An Airy beam is yet another exotic beam shape that can be generated through phase-only beam modulation. These beams have been introduced to optics relatively recently [11]. Like Bessel beams, Airy beams have intensity features that propagate in a diffraction-free manner. In addition, the dominant intensity features of Airy beams propagate along curved trajectories or accelerate. This self-bending property of Airy beams has been recently applied to the machining of curved cuts in silicon and diamond [12].

In this paper, we extend the family of exotic beam shapes applied to laser micromachining into the case of Bessel beams of higher order. These beams are hybrids of fundamental Bessel beams and optical vortices. Like vortex beams, Bessel beams of higher order carry orbital angular momentum that grows with the order of vorticity. The transverse intensity profiles of these beams comprise sets of concentric rings. The central ring has the highest peak intensity. Its radius grows with the order of the beam. The surrounding rings supply energy to the central ring on propagation, resulting in an extended diffraction-free propagation range through which the peak intensity of the central ring remains high. Using femtosecond higher-order Bessel beams, we experimentally demonstrate micromachining of ring-shaped ablation features on front surfaces of borosilicate glass slides. These features are produced through single-shot laser ablation. Multi-shot ablation of the front surface of a glass slide is shown to produce a pillar-like structure. We also investigate multi-shot laser machining of back surfaces of glass slides with

 

higher-order Bessel beams. Debris removal in that case is furnished by the immersion of the back side of the glass slide in water. Under certain conditions we observe azimuthal fragmentation of the initially smooth ring intensity features of the beams into individual filaments, due to self-focusing of higher-order Bessel beams either in water immediately adjacent to the back-side surface of the glass slide or inside the glass. Similar effects have been recently observed in a condensed medium (water) [13,14] and, at much higher intensities, in air [15,16]. Using higher-order Bessel beams allows for the machining of ring-shaped intensity features with high aspect ratios.

## 2. EXPERIMENTAL REALIZATION OF HIGHER-ORDER BESSEL BEAMS

The transverse amplitude distribution of the higher-order Bessel beam of order $n$ reads as follows:

$$E(\rho,\theta) = J_n(2\pi\rho/\rho_0)\exp(in\theta), \tag{1}$$

where $J_n$ is the $n$th-order Bessel function of the first kind, $n$ is the order of vorticity, and $(\rho,\theta)$ are transverse polar coordinates. A particular case with $n = 0$ corresponds to the fundamental Bessel beam [5]. For beams of the order higher than zero, the transverse intensity profiles of the beams comprise sets of concentric rings. The dominant intensity ring has the smallest diameter; for otherwise identical conditions, that diameter grows with the beam order $n$. In the absence of beam distortions, and in the nearly paraxial case, the on-axis intensity for these beams is close to zero.

A higher-order Bessel beam is generated through imposing a phase modulation in the form

$$\Phi(\rho,\theta) = -\alpha\rho + n\theta \tag{2}$$

onto an input collimated Gaussian beam, followed by the propagation of the beam into far-field or focusing the beam with a focusing lens or a focusing mirror, in which case the higher-order Bessel beam is realized in the vicinity of the focal plane of the focusing optic. In the above formula, the first term represents the axial part, which depends linearly on the beam radius. For higher values of the parameter $\alpha$, the transverse scale of the ring features of the resulting beams are smaller, but so is the longitudinal extent of the diffraction-free zone of the beam, and vice versa. The second term represents the azimuthal part. For the case $n = 0$, the azimuthal term is zero, corresponding to the fundamental Bessel beam. Typically, phase modulations of optical beams are produced through the application of phase masks or spatial light modulators (SLMs). As the maximum phase contrast attainable with spatial light modulators is limited, phase profiles are typically implemented modulo $2\pi$. An example of the modulo $2\pi$ phase distribution needed to produce a higher-order Bessel beam of the order 4 is shown in Fig. 1.

The fact that the phase profile imposed by an SLM is modulo $2\pi$ introduces quasi-periodicity in the phase modulation. As a result, several diffraction orders are produced which, in general, spatially overlap and interfere, resulting in distortions of the resulting beam pattern. An additional diffraction pattern results from the pixelated nature of the SLM. However, since pixels are usually very small (about 20 μm in our case), the corresponding diffraction orders are typically well separated and pose no problems. In order to cleanly separate the diffraction orders resulting from the modulo $2\pi$ modulation by the SLM, we add an additional phase term to the phase pattern that we wished to impose onto the beam. The additional term corresponds to an ordinary diffraction grating. An example of the resulting phase modulation is shown in Fig. 2. The additional grating term makes intervals over which the $2\pi$ steps occur smaller, resulting in a larger angular separation between the resulting diffraction orders. The orders become well separated and do not interfere. We select a particular diffraction order (typically the first order) and use it for producing desired phase modulations of the beam profile. A relay lens system is used after the SLM, and the undesirable diffraction orders are spatially separated and blocked in the Fourier plane of the relay system.

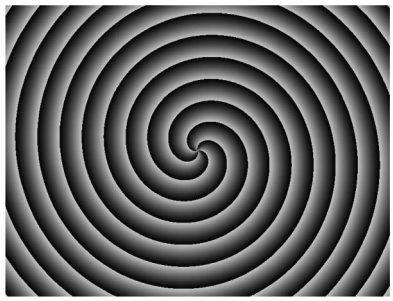

Fig. 1. Gray scale phase distribution needed for the generation of a Bessel beam of order 4. The phase is defined modulo $2\pi$.

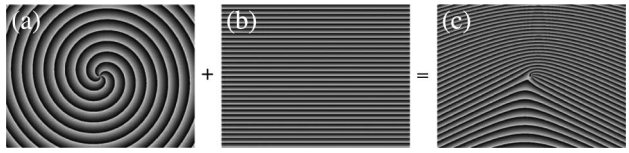


Fig. 2. (a) The desired phase pattern. (b) An ordinary grating term that is added to the phase pattern in order to separate different diffraction orders that result from the modulo $2\pi$ phase modulation by the SLM. (c) The resulting phase pattern imposed on the beam by the SLM. The first-order diffraction order is used for the generation of beams of interest; all other orders are removed by spatial filtering in the Fourier plane of an optical relay system.

## 3. EXPERIMENTS

The experimental setup used for the femtosecond laser micromachining with higher-order Bessel beams is schematically shown in Fig. 3. The laser source is a commercial Ti:sapphire laser system (Libra by Coherent). It outputs 65-fs-long pulses at a repetition rate of 1 kHz. The center wavelength of the laser pulses is 800 nm. The maximum energy per pulse attainable from the laser is 4 mJ, which is excessively large for the experiments reported here. The laser beam has a nearly perfect Gaussian shape. It is attenuated by a half-wave plate followed by reflection off a glass surface of a prism wedge. The angle of incidence on the surface of the wedge is made close to the Brewster's angle. The combination of the waveplate and the wedge is used to introduce adjustable attenuation, down to the nanojoule level, while maintaining the polarization of the attenuated laser beam. Spatial modulations of the transverse beam amplitude are produced through reflecting the beam off a computer-controlled

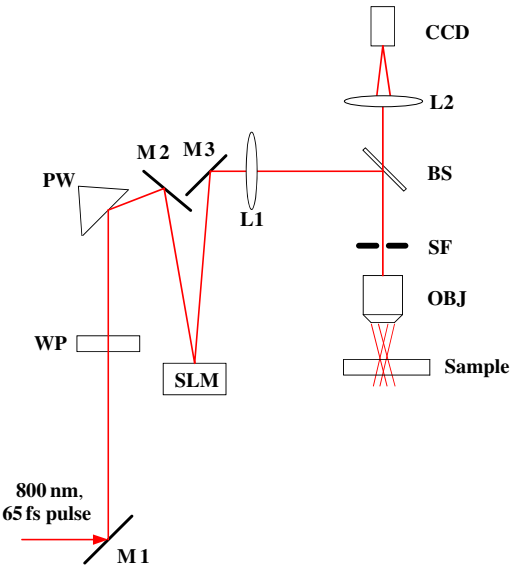


Fig. 3. Schematic of the experimental setup. M1, M2, and M3, mirrors; WP, half-wave plate; PW, prism wedge; SLM, spatial light modulator; L1, $f = 1$ m lens; BS, beam splitter; SF, spatial filter; OBJ, NA = 0.45 microscope objective; L2, $f = 10$ cm lens.

liquid-crystal-on-silicon spatial light modulator (LCOS-SLM by Hamamatsu Photonics). Spurious beam distortions due to interference of different diffraction orders, that are due to the modulo $2\pi$ beam modulation by the SLM, are eliminated by adding an additional diffraction-grating term to the phase profile, as discussed in the previous section. Not accounting for the variable loss introduced by the waveplate–wedge combination, the efficiency of transformation from the input beam into the shaped beam in our setup is about 30%. That loss is dominated by the finite diffraction efficiency into the first order of the added diffraction grating. Examples of the transverse intensity profiles of higher-order Bessel beams of several selected orders are shown in Fig. 4. These beam profiles are photographed by a CCD camera placed at the plane of the spatial filter, with the lens L1 removed.

The Fourier-transform lens L1 has a focal length of 1 m; it is placed 1 m away from the plane of the SLM. The first diffraction order is selected in the focal plane of L1, by spatial filtering, and focused by an infinity-corrected microscope objective with numerical aperture NA = 0.45. The resulting linear focus zone (Bessel zone) in the vicinity of the back focal plane of the objective is about 150 μm long. Samples that we machine with higher-order Bessel beams are borosilicate glass slides with the thickness of 150 μm. The samples are mounted on a computer-controlled linear motorized stage. By translating the stage transversely sufficiently fast, we can perform single-shot machining of our samples. The motorized stage is mounted on a manual XYZ micropositioning stage, so that either front or back surface of the sample can be placed at the position of the maximum intensity within the Bessel zone of the beam. The focusing condition is monitored through imaging the reflection off either front or back surface of the sample onto a CCD camera, using a beam splitter and an additional lens L2 with the focal length of 10 cm, as shown in Fig. 3. Experiments on front-surface machining discussed here are performed in both single-shot and multi-shot regimes. All back-surface machining experiments are multi-shot. In the latter case, the removal of the generated debris is furnished through the immersion of the back surface of the glass slide in a cell filled with water. Pulse energy is measured with a pyroelectric energy sensor. For visualizing the results of micromachining, the samples are sputter gold-coated and examined with a Hitachi S3400N scanning electron microscope.

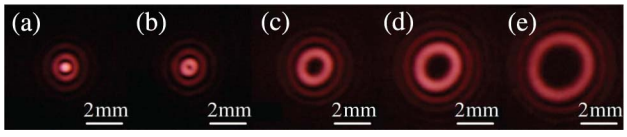


Fig. 4. Transverse intensity distributions of higher-order Bessel beams of orders (a) 0, (b) 1, (c) 4, (d) 6, and (e) 10.

## 4. RESULTS

For single-shot machining of front surfaces of borosilicate glass slides, we use higher-order Bessel beams of orders 4, 6, and 10. The motorized linear stage is translated at a rate of 40 mm/s which ensures single-shot illumination, with the separation between individual ablation sites, on the glass surface, by about 40 μm. Examples of so obtained ablation features are shown in Fig. 5. The exposure conditions are specified in the figure caption. In all cases shown the ablated features are doughnut-shaped, with the diameter that increases with the order of the beam, as expected. The ring features are smooth which is indicative of the high quality of the higher-order Bessel beams produced in our setup.

In the case of multi-shot front-surface machining, a micropillar structure can be fabricated under certain conditions.

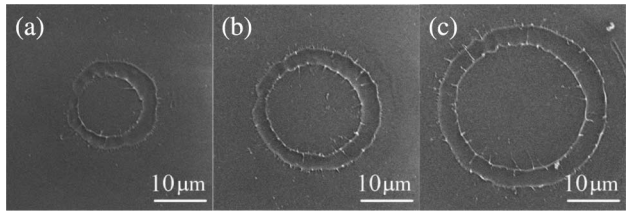


Fig. 5. Ablation marks produced by front surface single-shot machining using higher-order Bessel beams of orders (a) 4, (b) 6, and (c) 10. Specific values of pulse energy incident on the sample are chosen to produce clear ablation features. For the cases shown, the pulse-energy values are (a) 16 μJ, (b) 18 μJ, and (c) 20 μJ.

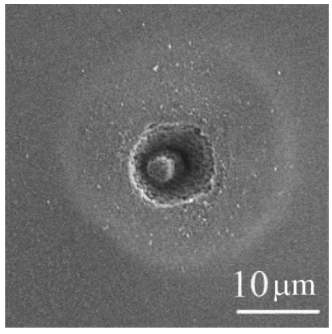


Fig. 6. Front surface multi-shot processing by a Bessel beam of order 4, with energy per pulse of 8 μJ and exposure time of about 10 s (corresponding to about 10,000 laser shots).

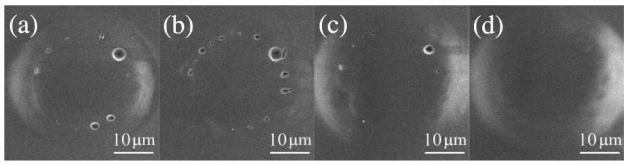


Fig. 7. Back-surface multi-shot machining using higher-order Bessel beam of order 4. In each case shown, the ablation sites are exposed to about 60,000 laser shots. Different cases correspond to different values of energy per laser pulse: (a) 10 μJ, (b) 12 μJ, (c) 14 μJ, and (d) 16 μJ. For the first case shown, the azimuthal pulse breakup of the ring intensity feature occurs near the glass–water interface. For higher values of pulse energy, the azimuthal breakup occurs deeper inside the glass sample, and the beaded ablation feature on the glass surface disappears.

An example is shown in Fig. 6. In the case shown, the pulse energy on the sample was 8 μJ, and the ablation site was exposed to about 10,000 laser pulses (corresponding to 10 s exposure time). The asymmetry in the appearance of the feature is likely to be caused by the distortion of the beam pattern used to produce that feature. The beam distortion is evident in the single-shot ablation mark produced by the same beam and shown in Fig. 5(a).

For multi-shot back-surface ablation experiments, we use a higher-order Bessel beam of order 4. In all cases, ablation sites were illuminated for about 1 min, corresponding to the exposure to about 60,000 laser shots. We found that in that case, instead of smooth ring-shaped ablation features, laser machining produced ring-shaped features fragmented into individual discrete spots, as shown in Fig. 7. We hypothesize that the observed ring fragmentation is due to the azimuthal modulation instability caused by self-focusing of the higher-order Bessel beam inside the glass or in water immediately adjacent to the glass–water interface. This conclusion is supported by the observation that the ablation feature on the back surface disappears if the pulse energy is increased by about 60%, while keeping the exposure time constant. In that case, the azimuthal breakup of the ring intensity feature occurs deeper inside the glass, distorting the subsequent propagation of the beam. Similar behavior of higher-order optical vortices has been experimentally observed in a condensed medium (water) [13,14] and, at a significantly higher power, in air [15,16].

We estimate that in our focusing geometry, about 70% of the beam energy is confined within the dominant ring feature of the higher-order Bessel beam of order 4, while the rest of the beam energy is carried by the surrounding concentric ring structure. For the case of pulse energy of 10 μJ, the peak power of the dominant ring feature of the beam is about 110 MW. The critical power for self-similar collapse of a continuous-wave vortex beam of order 4 can be estimated as $P_{cr}^{(4)} \approx 2\sqrt{3} \times 4 \times P_{cr}^{(0)}$ [17], where $P_{cr}^{(0)}$ is the critical power for self-focusing collapse of a Gaussian beam. (A vortex self-focuses self-similarly if it maintains its doughnut-shaped intensity feature, without it fragmenting into individual filaments.) At 800 nm wavelength, in glass, $P_{cr}^{(0)} \approx 2.5$ MW [18], thus $P_{cr}^{(4)} \approx 35$ MW. It has been shown experimentally that the azimuthal breakup of ring intensity features of vortex beams precedes self-similar collapse [13,16]. Thus, in our case of the higher-order Bessel beam of order 4, with peak power of the dominant ring intensity feature of 110 MW, the power significantly exceeds the threshold for azimuthal ring breakup into individual filaments.

## 5. CONCLUSION

In conclusion, we have experimentally investigated micromachining of borosilicate glass slides with femtosecond Bessel beams of higher order. Higher-order Bessel beams extend the family of beams that can be conveniently produced from Gaussian beams through phase-only beam-front modulation. Extended linear focus zones of these beams facilitate machining geometries with large working distances and high aspect ratios. Both front-surface and back-surface machining have been experimentally investigated. In the latter case, debris removal was furnished through the immersion of the back sides of the glass slides in water. We have observed azimuthal fragmentation of the smooth ring intensity features of higher-order Bessel beams into individual filaments, due to self-focusing. When the fragmentation occurs near the glass–water interface, it results in the production of distinct point-like ablation features populating the dominant intensity ring of the beam. Increasing pulse energy drives the fragmentation deeper inside the glass material, and the point-like features on the back surface of the glass slide disappear. In the case of multi-shot front-surface machining, a pillar-like structure can be fabricated.

## ACKNOWLEDGMENTS

This work was supported by the U.S. Air Force Office of Scientific Research (AFOSR) through grants FA9550-12-1-0143 and FA9550-12-1-0482 and by the U.S. Defense Threat Reduction Agency (DTRA) through grant HDTRA 1-14-1-0009. We thank Dr. Tom D. Milster and Mr. Victor Densmore III for assistance with operating the electron microscope and Dr. Ming Zhao and Mr. Han Zhang for helpful discussions.

## REFERENCES

1. G. M. Whitesides, "The origins and the future of microfluidics," Nature **442**, 368–373 (2006).
2. L. B. Fletcher, J. J. Witcher, N. Troy, S. T. Reis, R. K. Brow, and D. M. Krol, "Direct femtosecond laser waveguide writing inside zinc phosphate glass," Opt. Express **19**, 7929–7936 (2011).
3. M. Hong, B. Luk yanchuk, S. Huang, T. Ong, L. Van, and T. Chong, "Femtosecond laser application for high capacity optical data storage," Appl. Phys. A **79**, 791–794 (2004).
4. J. H. McLeod, "The axicon: a new type of optical element," J. Opt. Soc. Am. **44**, 592 (1954).
5. J. Durnin, J. J. Miceli, and J. H. Eberly, "Diffraction-free beams," Phys. Rev. Lett. **58**, 1499–1501 (1987).
6. M. K. Bhuyan, F. Courvoisier, P. A. Lacourt, M. Jacquot, R. Salut, L. Furfaro, and J. M. Dudley, "High aspect ratio nanochannel machining using single shot femtosecond Bessel beams," Appl. Phys. Lett. **97**, 081102 (2010).
7. L. Allen, M. W. Beijersbergen, R. J. C. Spreeuw, and J. P. Woerdman, "Orbital angular momentum of light and the transformation of Laguerre–Gaussian laser modes," Phys. Rev. A **45**, 8185–8189 (1992).
8. T. Kuga, Y. Torii, N. Shiokawa, T. Hirano, Y. Shimizu, and H. Sasada, "Novel optical trap of atoms with a doughnut beam," Phys. Rev. Lett. **78**, 4713–4716 (1997).
9. L. Paterson, M. P. MacDonald, J. Arlt, W. Sibbett, P. E. Bryant, and K. Dholakia, "Controlled rotation of optically trapped microscopic particles," Science **292**, 912–914 (2001).
10. C. Hnatovsky, V. G. Shvedov, W. Krolikowski, and A. V. Rode, "Materials processing with a tightly focused femtosecond laser vortex pulse," Opt. Lett. **35**, 3417–3419 (2010).
11. G. A. Siviloglou, J. Broky, A. Dogariu, and D. N. Christodoulides, "Observation of accelerating Airy beams," Phys. Rev. Lett. **99**, 213901 (2007).

12. A. Mathis, F. Courvoisier, L. Froehly, L. Furfaro, M. Jacquot, P. A. Lacourt, and J. M. Dudley, "Micromachining along a curve: femtosecond laser micromachining of curved profiles in diamond and silicon using accelerating beams," Appl. Phys. Lett. **101**, 071110 (2012).
13. L. T. Vuong, T. D. Grow, A. Ishaaya, A. L. Gaeta, G. W. 't Hooft, E. R. Eliel, and G. Fibich, "Collapse of optical vortices," Phys. Rev. Lett. **96**, 133901 (2006).
14. S. Shiffler, P. Polynkin, and J. Moloney, "Self-focusing of femtosecond diffraction-resistant vortex beams in water," Opt. Lett. **36**, 3834–3836 (2011).
15. A. Vincotte and L. Berge, "Femtosecond optical vortices in air," Phys. Rev. Lett. **95**, 193901 (2005).
16. P. Polynkin, C. Ament, and J. V. Moloney, "Self-focusing of ultraintense femtosecond optical vortices in air," Phys. Rev. Lett. **111**, 023901 (2013).
17. G. Fibich and N. Gavish, "Critical power of collapsing vortices," Phys. Rev. A **77**, 045803 (2008).
18. T. A. Pitts, T. S. Luk, J. K. Gruetzner, T. R. Nelson, A. McPherson, S. M. Cameron, and A. C. Bernstein, "Propagation of self-focusing laser pulses in atmosphere: experiment versus numerical simulation," J. Opt. Soc. Am. B **21**, 2008–2016 (2004).